

# Functional Graph Alterations in Schizophrenia: A Result from a Global Anatomic Decoupling?

## Authors

J. Cabral<sup>1,2</sup>, M. L. Kringelbach<sup>2,3</sup>, G. Deco<sup>1,4</sup>

## Affiliations

<sup>1</sup>Theoretical and Computational Neuroscience Group, Center for Brain and Cognition, Universitat Pompeu Fabra, Barcelona, Spain

<sup>2</sup>Department of Psychiatry, University of Oxford, Oxford, U.K.

<sup>3</sup>Center of Functionally Integrative Neuroscience (CFIN), Aarhus University, Aarhus, Denmark

<sup>4</sup>Institut Català de Recerca i Estudis Avançats, Barcelona, Spain

## Key words

- computational model
- structural connectivity
- functional network
- graph theory
- schizophrenia

## Abstract

**Introduction:** During rest, the brain exhibits slow hemodynamic fluctuations (<0.1 Hz) that are correlated across spatially segregated brain regions, defining functional networks. Resting-state functional networks of people with schizophrenia were found to have graph properties that differ from those of control subjects. Namely, functional graphs from patients exhibit reduced small-worldness, increased hierarchy, lower clustering, improved efficiency and greater robustness. Notably, most of these parameters correlate with patients' cognitive performance. **Methods:** To test if a brain-wide coupling deficit could be at the origin of such network reorganization, we use a model of resting-state

activity where the coupling strength can be manipulated. For a range of coupling values, the simulated functional graphs obtained were characterized using graph theory.

**Results:** For a coupling range, simulated graphs shared properties of healthy resting-state functional graphs. On decreasing the coupling strength, the resultant functional graphs exhibited a topological reorganization, in the same way as described in schizophrenia.

**Discussion:** This work shows how complex functional graph alterations reported in schizophrenia can be accounted for by a decrease in the structural coupling strength. These results are corroborated by reports of lower white matter density in schizophrenia.

## Introduction

The cognitive and behavioural symptoms of people with schizophrenia are hypothesized to involve a disruption of neuronal interactions resulting in dysfunctional cognitive integration [1,2]. This hypothesis is supported by reports of abnormal temporal correlations of neural activity in the disease [3–5], possibly related to deficient synaptic plasticity [6], dopaminergic [7,8] and cholinergic [9,10] malfunctions, or even to a decrease in white matter anatomic connections [11–14]. Assessing functional connectivity between segregated brain regions in terms of temporal correlations between blood oxygenation level dependent signals (BOLD) detected with functional MRI (fMRI), has revealed a topological organization of brain activity during rest, which is intrinsically related to the underlying anatomic structure [15–17]. These functional connections yield so-called resting-state functional networks. In a recent study from Lynall and colleagues [18], resting-state functional networks from healthy controls and people with

schizophrenia have been characterized using measures from graph theory. This method has shown clinical relevance by exposing significant differences between patients and controls. In particular, the functional networks from people with schizophrenia were found to be less small-world, more hierarchical, less clustered, more efficient and more robust. In addition, the probability of both low- and high-degree hubs was decreased in patients. Interestingly, most of these topological metrics were found to be correlated with a verbal fluency score, suggesting a link between the properties of functional networks and the performance of cognitive integration. Several studies of brain connectivity have shown that functional connectivity depends strongly on the underlying anatomic structure [19]. But are the functional graph measures exclusively dependent on the static wiring diagram of the anatomic network? Is it necessary to have topological alterations in the anatomic network to give rise to the functional network reorganization described in schizophrenia?

## Bibliography

DOI <http://dx.doi.org/10.1055/s-0032-1309001>  
 Pharmacopsychiatry 2012; 45 (Suppl. 1): S57–S64  
 © Georg Thieme Verlag KG  
 Stuttgart · New York  
 ISSN 0176-3679

## Correspondence

### J. Cabral

Theoretical and Computational Neuroscience Group  
 Center for Brain and Cognition  
 Universitat Pompeu Fabra  
 C/Roc Boronat 138  
 08018 Barcelona  
 Spain  
 joana.cabral@upf.edu



At the anatomic level, the pathology of schizophrenia has been related to a wide range of anatomic abnormalities, including ventricular enlargement, associated with anomalous neurodevelopment or neurodegenerative alterations [20]. Importantly, schizophrenia is likely to be the result of both general and specific localized changes in both grey and white matter [21,22]. However, a crucial missing point is to consider the impact of these anatomic changes on the emergence of functional network dynamics (e.g., during rest).

Notably, several studies report correlations between the strength of anatomic connectivity, inferred from the degree of fractional anisotropy, and behavioural measures in schizophrenia [11,23,24]. In the present work, disrupted functional networks in schizophrenia are hypothesized to be related to a decreased coupling between cortical regions. To validate this hypothesis we use a computational model to investigate the impact of a global decoupling in the properties of emergent functional networks. Note that this decoupling encompasses either anatomic white matter reduction or neuromodulator-based affected neurotransmission. We model resting-state functional connectivity using a model of ongoing brain activity previously proposed by Cabral and colleagues [25]. The model consists of a network of gamma-frequency oscillators, where each oscillator represents a given anatomic region. The coupling architecture was derived from the brain's anatomic connectome. Importantly for this work, a global parameter scales the coupling strength between brain regions. The neuronal activity at each brain region was simulated and the signal transformed into a hemodynamic response to simulate a resting BOLD signal. From the simulated BOLD time-courses, functional graphs were constructed following the methodology from Lynall and colleagues [18] for a reliable comparison.

The graph-theoretical measures of emergent functional graphs were found to vary with the coupling strength. For a range of coupling strengths, simulated functional graphs had properties similar to those reported in healthy resting-state functional graphs. Moreover, on decreasing the coupling strength, simulated functional graphs exhibit an increase in efficiency, hierarchy and robustness and a decrease in small-worldness, clustering and degree variance, in the same way as described in schizophrenia. Overall, these results show that the functional network alterations underlying schizophrenia are not necessarily caused by an alteration in the static topology of the underlying anatomic architecture. Indeed, as shown here, the same anatomic structure followed by a global decrease in the connection weights can lead to the emergence of functional networks with distinct graph properties, which could be hypothetically related to either a white matter connectivity deficit and/or to deficient neurotransmission, as reported in schizophrenia. Moreover, these results go beyond schizophrenia, suggesting a link between anatomic decoupling and decreased cognitive integration.

## Methods

### Anatomic brain network

Anatomic brain networks were constructed using diffusion tensor imaging (DTI) from the brains of 21 healthy, normal participants (11 males and 10 females, age: 22–45 years) scanned on the same Philips Achieva 1.5 Tesla MRI system [26]. Diffusion MRI was acquired by using a single-shot echo planar imaging-based sequence with coverage of the whole brain; repetition time (TR), 9390 ms; echo time (TE), 65 ms. DTI images utilized 32 optimal non-linear diffusion weighting

directions ( $b=1200\text{s/mm}^2$ ) and 2 non-diffusion weighted volumes; reconstructed matrix= $128\times 128\times 45$ ; reconstructed voxel size  $2.0\text{mm}\times 2.0\text{mm}\times 2.0\text{mm}$ . We also acquired  $T_1$ -weighted structural images.

The automated anatomic labelling (AAL) template was used to parcellate the entire brain in native DTI space into 90 cortical and subcortical regions (45 for each hemisphere), where each region represents a node of the brain network [27]. The AAL masks were brought into MNI space by using Flirt (FSL, Oxford) [28] to co-register the  $b_0$  image in diffusion MRI space to the  $T_1$ -weighted structural image and then to the  $T_1$  template of ICBM152 in MNI space [29]. Interpolation using the nearest-neighbour method was used to ensure that discrete labelling values were preserved.

We used the Fdt toolbox in FSL (<http://www.fmrib.ox.ac.uk/fsl/>, Oxford) to process the diffusion MRI in the standard way using the probtrackx algorithm [30,31]. We calculated the connectivity probability from each seed region to the 89 other brain regions (using in-house Perl scripts). Connectivity probability was found by applying probabilistic tractography using a sampling of 5000 streamline fibres per voxel. The connectivity probability from the seed voxel  $i$  to another voxel  $j$  was defined by the number of fibres passing through voxel  $j$  divided by the total number of fibres sampled from voxel  $i$  [31]. This was then extended from the voxel level to the level of each region, i.e., in a seed brain region consisting of  $n$  voxels,  $5000\times n$  fibres were sampled. The connectivity probability from the seed region to a given region is the number of fibres passing through a given region divided by  $5000\times n$ . The un-directional connectivity probability  $P_{ij}$  was estimated by averaging the probabilities from  $i$  to  $j$  and from  $j$  to  $i$ , which are highly correlated across the brain for all subjects ( $r=0.70$ ,  $p<10^{-50}$ ).

We constructed a weighted network by defining a distance/weight associated with each edge. Specifically, we computed  $W_{ij}=1-P_{ij}$  as the distance/weight between brain region  $i$  and  $j$ , as used in previous literature [32]. Please note that the distance/weight here does not correspond to a physical length. For each subject, a  $90\times 90$  symmetrically weighted cortical network was constructed, representing the anatomic organization of the cerebral cortex. Networks were averaged across subjects and regions connected with less than 1% of possible connections were considered to be disconnected.

### Model of resting-state functional connectivity

The dynamics of each node, representing a brain region, was modelled in a reduced way as a phase oscillator  $\theta_n$  with an intrinsic frequency  $\omega_0$  in the gamma range (here  $\omega_0=40\text{Hz}$ ) [25]. The gamma-frequency oscillations represent the firing-rate oscillations emerging spontaneously from neural populations with a moderate level of synchrony, as described in a number of experimental and theoretical studies [33–36]. The interaction between regions was computed using the Kuramoto model of coupled oscillators with time delays [37]:

$$\frac{d\theta_n}{dt} = \omega_0 + k \sum_{p=1}^N C_{np} \sin(\theta_p(t - \tau_{np}) - \theta_n(t)), n = 1, \dots, N.$$

The time delays  $\tau_{np}$  correspond to the axonal conduction time (here  $\langle \tau \rangle = 20\text{ms}$ ) and were defined as a function of the transmission speed and the Euclidean distance between the centres of gravity of regions  $n$  and  $p$ .

Simulations of resting-state neuronal activity were run for 300 s ( $\Delta t=0.1\text{ms}$ ) for a range of coupling strengths ( $k=0, \dots, 15$ ). The



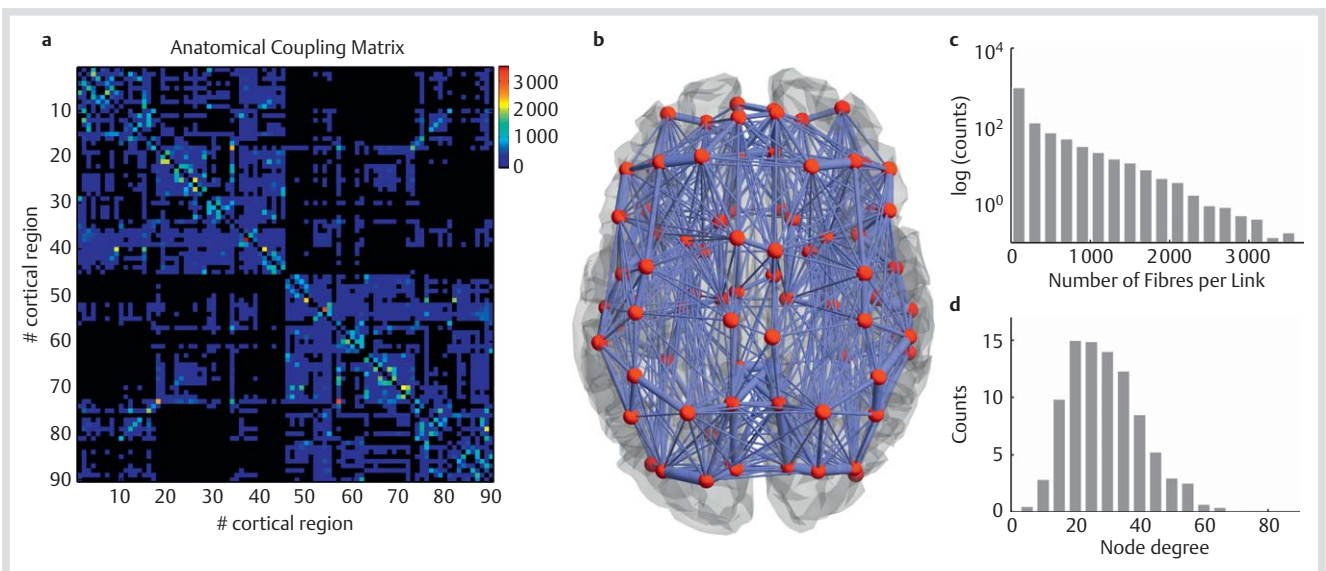


**Fig. 1** Anatomic brain network derived from DTI. **a** The connectivity matrix indicates the average number of fibres detected between any pair of regions defined according to the AAL parcellation across the 21 normal subjects (see [Table S1](#) for the names of the regions). **b** Representation of the network, where nodes (red) are located at the centre of each region and the thickness of the links is proportional to the number of fibres detected between nodes. **c** Histogram of the number of fibres per pairwise connection and **d** node degree histogram both averaged across participants.

signal was then transformed into hemodynamic fluctuations using the Balloon-Windkessel model [25,38]. For each value of coupling strength, the functional connectivity matrix was computed as correlation matrix of hemodynamic fluctuations. The dynamics of the network was evaluated by the order parameter  $R(t)$  given by the following equation:

$$R(t) = \left[ \frac{1}{N} \sum_{n=1}^N e^{i\theta_n(t)} \right]$$

$R$  measures phase uniformity and varies between 0 for a fully desynchronized – or incoherent – state and 1 for a fully synchronized state. We characterized the network dynamics by the mean synchronization level  $\bar{R}$  and the standard deviation  $\sigma_R$  of the order parameter  $R$  over the simulated time interval.  $\sigma_R$  indicates the degree of metastability of the network [39].

We applied principal component (PC) analysis to the covariance matrix of the simulated BOLD signal to obtain a measure of “global integration”, calculated as the ratio of the first eigenvalue to the sum of all the others: [40].

$$I = \lambda_1 / \sum_{j=2}^N \lambda_j$$

### Graph theoretical analysis of simulated functional networks

The set of synthetic functional networks generated with the use of the computational model was characterized using graph theory. To evaluate functional networks by means of graph theory, the correlation matrix of BOLD responses needs to be binarized into a graph ( $G_{ij}$ ), where correlations above a certain threshold are set to 1 and 0 otherwise. In order to compare the properties of simulated functional networks with the values reported by Lynall and colleagues [18], we selected the same 72 AAL regions considered in that work, discarding the remaining 18 subcortical regions ([Table S1](#)), and applied the same thresholding technique to the correlation matrices. In more detail, from each functional connectivity matrix, 14 binary graphs were derived by thresholding to connection densities ranging from 37 to 50%

with a 1% increment. Each of these graphs was characterized using global graph measures and the values reported correspond to the average across the 14 graphs obtained from each single functional connectivity matrix. The following graph measures were considered (See *Supplementary Information* for details):

**Efficiency:** It is the inverse of the characteristic path length of a graph [41]. The lesser the number of paths linking any pair of nodes, the higher the efficiency of the graph.

**Clustering:** It indicates the probability of 2 nodes that are coupled to a third region, being also coupled to one another, forming triangles.

**Hierarchy:** It evaluates the relationship between the number of connections in one node (node degree) and its clustering degree [42,43]. The hierarchy is higher if nodes with more connections (hubs) are also poorly clustered.

**Small-worldness:** A network is small world if high clustering degree coexists with high efficiency [44].

**Robustness to attacks:** It indicates the network’s resilience in keeping connectedness when nodes are removed either randomly (random attack) or sorted in descending degree (targeted attack).

**Degree distribution parameters:** The degree of a node is simply given by the number of connections it maintains with other nodes. The degree distribution was characterized by its variance and by 2 parameters, the power exponent  $\alpha$  and the lower exponential degree cut-off  $d_c$ , found to optimally fit the distribution to a gamma function ( $P(d) = Nd^{\alpha-1} \exp(-d/d_c)$ ) [18]. Degree distribution measures were estimated only for graphs with 37% connection cost.

Graph measures were evaluated using the Brain Connectivity Toolbox [45] and the MatlabBGL Toolbox (Gleich, 2006).



## Results

### Properties of the anatomic network

The 21 anatomic networks obtained from 21 healthy participants (11 males and 10 females, age: 22–45 years) have an average connection density of 32%. Each connection (link) is composed by around 208 fibres. However, between some pairs of brain regions, up to 3000 fibres have been detected (see the histogram in **Fig. 1c**). From the degree distribution shown in **Fig. 1d**, we can see that each region is connected to an average of 25 other regions and this distribution is quite homogeneous (bell-shaped).

In addition, the anatomic networks were characterized by means of graph theory (**Table 1**). Anatomic networks were found to be “small-world” (small-worldness >1), which means that networks are not only efficient (short average path length) but also highly clustered when compared with an equivalent random graph. In addition, the networks have a positive hierarchy, meaning that high degree nodes – or hubs – are the less clustered and vice versa. Furthermore, networks were found to be robust to either random or targeted attack ( $r \approx 1$ ), maintaining strong connectedness as nodes are removed either randomly or by descending node degree.

### Dynamics of simulated spontaneous activity as a function of the coupling strength

The dynamics of simulated brain activity varies as a function of the coupling strength. As observed in **Fig. 2a**, for weak couplings, the phases are almost completely desynchronized, and the order parameter is close to zero. As the coupling increases, regions become more and more synchronized with each other.

**Table 1** Properties of the anatomic network (mean  $\pm$  1 standard deviation across 21 subjects).

Connection density (%):	32.7 $\pm$ 4.6	Small-worldness:	1.96 $\pm$ 0.20
Fibres/connection:	208 $\pm$ 17	Hierarchy:	0.139 $\pm$ 0.016
Global efficiency:	0.65 $\pm$ 0.03	Robustness (random):	0.993 $\pm$ 0.008
Average clustering:	0.64 $\pm$ 0.02	Robustness (targeted):	0.9244 $\pm$ 0.02

In the region between incoherence and synchrony ( $0 < k < 10$ ), the metastability index is high (**Fig. 2b**), indicating that the network is in a non-stationary regime, where the order parameter fluctuates in time due to meta-stable synchronized clusters. As described in Cabral et al. [25], the metastability is important to generate low frequency fluctuations in brain activity. However, above a certain coupling value (i.e.,  $k > 13$ ) the neuronal oscillations become too synchronized and the metastability index is brought down to zero. In that case, slow fluctuations disappear. This explains why, above this critical coupling value, functional networks become less globally integrated and less globally correlated (**Fig. 2c, d**). Furthermore, we report the correlation between anatomic connectivity (AC) and simulated BOLD functional connectivity (FC). As expected, it is in the region of metastability that the functional networks are shaped by the underlying anatomic structure [25].

### Graph-theoretical properties of emergent functional networks

The topological organization of synthetic functional networks was found to vary as a function of the coupling strength (**Fig. 3**). Some parameters from graph theory, namely the average clustering, the small-worldness and the variance of the degree distribution, were found to decrease as the coupling weights became weaker, while others such as the hierarchy, the global efficiency and the robustness increased as the regions became more disconnected. These alterations mean that, when the connectivity between brain regions is deficient, the emergent patterns of functional connectivity tend to be slightly randomized, with less clustered structure and fewer low- and high-degree nodes.

If the coupling is too weak, the spontaneous dynamics is in an incoherent regime and the functional connectivity strength is low (**Fig. 2a, d**). The resulting functional networks share properties of random networks. As shown in **Fig. 3**, for low  $k$  the small-world index is close to 1 which means that the clustering coefficient and the efficiency of the networks are similar to those of comparable random graphs. The fact that these networks exhibit a higher efficiency is related to the increase of random connections, which consequently decrease the average shortest path length. In addition, since highly connected nodes (or hubs) are less probable in random networks, it is expected

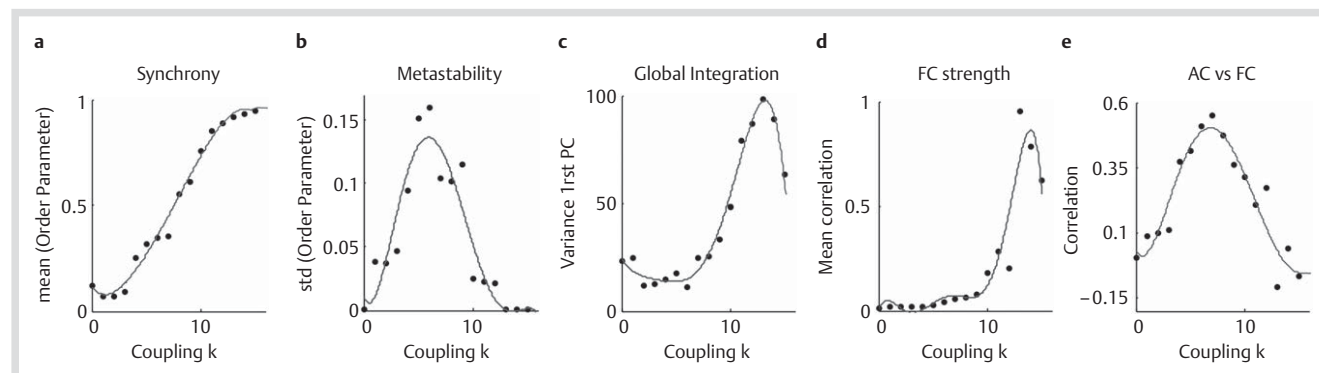


**Fig. 2** Dynamics of simulated spontaneous activity as a function of the coupling strength  $k$ . **a** The mean synchrony degree varies from desynchrony ( $\langle R \rangle \approx 0$ ) to full synchrony ( $\langle R \rangle \approx 1$ ). In **b** the standard deviation of the order parameter indicates the metastability of the system is higher in the intermediate region between desynchrony and synchrony. **c** The variance of the first PC also increases with the coupling strength, meaning

that the BOLD signals become more globally integrated. **d** The functional connectivity strength, measured as the average correlation between simulated BOLD signals, increases together with the global integration. **e** The correlation between the anatomical and the functional connectivity is increased in the metastability region (AC = anatomic connectivity and FC = functional connectivity).

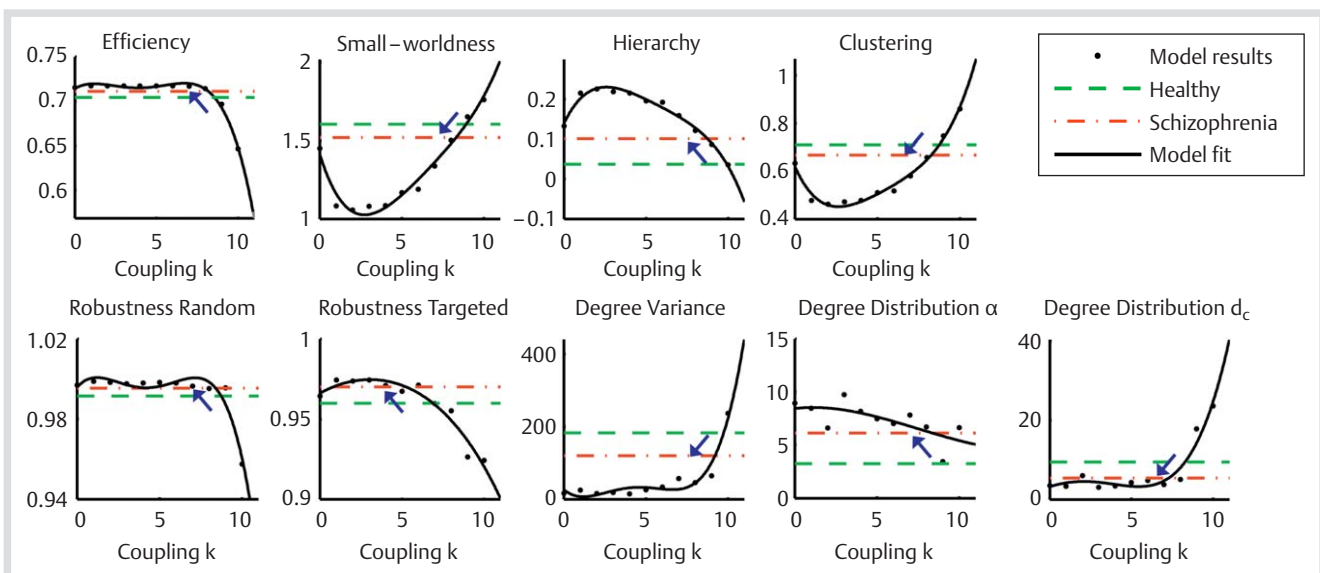


**Fig. 3** Properties of simulated functional networks as a function of the coupling strength  $k$ . In this figure we report a number of measures from graph-theory (black dots) for coupling strength values ranging from 0 to 10 (above that value networks become too correlated, with consequent loss of realism). The measures vary as a function of  $k$ : solid lines show the fit to fourth order polynomial functions. For reference, the measures

reported experimentally for resting-state functional graphs from healthy controls and schizophrenia patients [18] are indicated as green dashed lines and red dotted lines, correspondingly. The blue arrows indicate the decrease or increase of the respective graph-theoretical measurements as the coupling is decreased, emulating the passage from health to schizophrenia.

that degree distributions become narrower and bell-shaped. These networks, however, are more robust to attacks, either random or targeted, because the probability of hitting a hub when removing a node is decreased. Please note that a higher robustness or a higher efficiency are general properties of random networks, and are not by themselves advantageous for an optimal cognitive integration. Therefore, these values are expected to be lower in the functional organization of resting-state brain activity from healthy controls.

As the coupling weights are increased in the model, the organizational properties of the resulting synthetic networks evolve towards values characteristic of functional networks from healthy brains (reported as green dashed horizontal lines). The simulated graphs exhibit higher small-worldness, the clustering coefficient increases and the degree distribution is wider with higher probability of high degree hubs. Interestingly, the organizational properties of functional graphs from people with schizophrenia (red dashed horizontal lines) are generally found in-between graphs from healthy people and more random graphs, suggesting a subtle randomization of functional networks in schizophrenia. Results show that this randomization can be induced by a global decrease in the coupling between brain regions, while the static topological properties of the anatomic network remain unchanged.

## Discussion

Overall, the results reported herein show that the graph properties of functional networks derived by the model are sensitive to the coupling strength. Notably, a small decrease in the global coupling strength can give rise to the same type of network reorganization as found in the functional graphs of people with schizophrenia with respect to controls [18]. Despite its simplicity, the model adds

a new perspective from dynamic systems to explain the functional network alterations found in schizophrenia.

Functional graphs obtained at lower coupling are more random, as indicated, for example, by a lower small-world index or a higher robustness. This randomization, hypothetically led by a slight brain-wide disconnection, has an impact on the capacity of information integration of functional networks. Indeed, as described in Lynall et al. [18], this type of topological organization of functional networks has shown a negative correlation with the verbal fluency from participants.

The decoupling hypothesis presented herein implies that neural transmission is affected in the disease. This disrupted coupling between regions could be due to either axonal or synaptic mechanisms, supported on one side by reports of significant decreased anatomic connectivity in patients relative to controls [11–14] or by findings of damage occurring at the synaptic level, associated to a deficient modulation of synaptic plasticity [46,47] and/or dopaminergic [7,8], cholinergic [9,10], or glutamatergic [48] malfunctions in schizophrenia. Importantly, the mechanisms leading to a decreased coupling strength are not necessarily exclusive and could coexist [47]. In addition, for generalization, we assumed a widespread decrease in coupling across the whole brain. However, these results could be extended in the future to include the hypothesis of localized changes in the anatomic structure [21,22].

In the model, synthetic functional networks acquire the shape of the human resting-state functional networks when the dynamics is meta-stable, which means that the system is neither fully synchronized nor totally desynchronized, but partially synchronized states occur sporadically in time. In this meta-stable state, fluctuations in the order parameter give rise to positive correlations at low frequencies among regions. In a previous work from our group [25], this meta-stable regime was proposed to be at the origin of healthy resting-state fMRI functional connectivity.



Although we have shown that a weak decoupling could be at the origin of altered resting state functional networks in schizophrenia, the origin of this decoupling still needs to be validated. Indeed, whether reduced functional connectivity between cortical regions results from a deficient synaptic neurotransmission [8–10] or from an reduction in anatomic white matter connectivity [11–14] remains an open issue.

Future work will be directed in order to study the organization of resting-state functional networks in other mental illnesses beyond schizophrenia, such as Alzheimer's disease, where a subtle randomization of resting-state patterns has also been reported [49].

## Appendix

### Functional Graph Alterations in Schizophrenia: A Result from a Global Anatomic Decoupling?

J. Cabral, M. L. Kringelbach, G. Deco

#### Generating Graphs from Correlation Matrices

Correlation matrices have values ranging between  $-1$  and  $1$ . To study these weighted matrices by means of graph theory, they need to be binarized. This means that the correlation matrix is transformed into a matrix  $G$  with only zeros and ones, i.e.,  $G_{ij} = 1$  when the correlation between node  $j$  to node  $i$  is higher than a certain threshold, and  $G_{ij} = 0$  otherwise. Note that the same correlation matrix can be transformed into distinct binary graphs, depending on the threshold defined. In Supplementary (Fig. S1), we show how the same functional connectivity matrix (obtained from correlating the BOLD signals from all 90 regions) can give distinct binary graphs, depending on the connection density desired.

#### Degree

The degree of a node in a graph is defined as the number of edges connecting that node to the network using.

$$d_i = \sum_j A_{ij}$$

## Acknowledgements

The research reported herein was supported by the Portuguese Foundation for Science and Technology SFRH/BD/36730/2007, by the TrygFonden Charitable Foundation, by the Brain Network Recovery Group through the James S. McDonnell Foundation, by the European Union grants "Brainsync" and "BrainScales", by the Spanish Research Project SAF2010-16085, by the Foundation "La Marató", by the CONSOLIDER-INGENIO 2010 Program CSD2007-00012.

## Disclaimer

The authors declare no conflict of interest.

The degree distribution is given as the probability distribution of node degrees over the whole network [50].

## Efficiency

The global efficiency of a graph  $E(G)$  is estimated by calculating inverse of the mean shortest path length:

$$E = \frac{1}{N-1} \sum_{j \neq i} \frac{1}{l_{ij}}$$

where  $l_{ij}$  is the shortest path length between node  $i$  and node  $j$  in  $G$  [41].  $E(G)$  attains its maximal value, 1, for a fully connected graph.

## Average Clustering

The average clustering of a graph  $C(G)$  indicates the tendency of its nodes to cluster together and is given by the average of the nodes clustering coefficients  $C_i$ . For undirected graphs,  $C_i$  is the ratio of the number of edges between the neighbors of a node and the total number of possible edges between these neighbors. Noting  $V_i$  the subset of nodes connected to node  $i$ , the clustering coefficient was calculated as follows:

$$C_i = \frac{1}{d_i(d_i-1)} \sum_{j,k \in V_i, k \neq j} A_{jk}$$

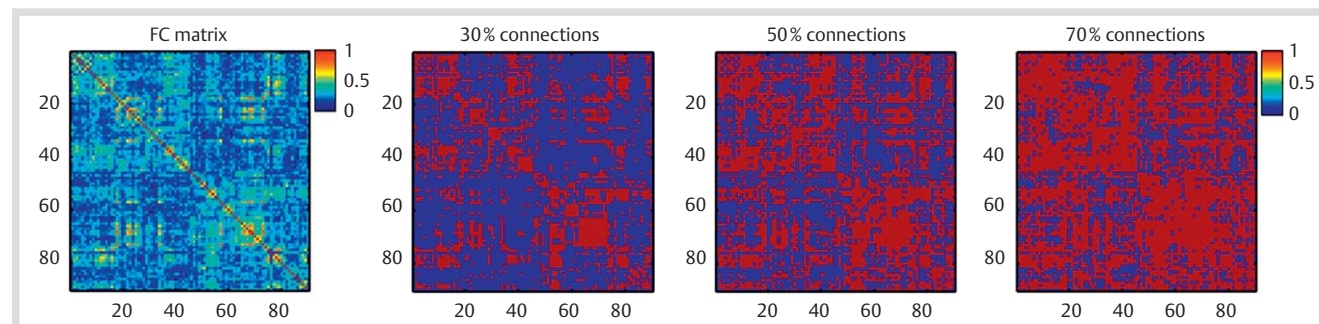


**Fig. S1** Thresholding functional connectivity (FC) matrices into graphs with distinct connection densities. Here we use an FC matrix obtained from simulations with  $k = 0.8$ .



**Table S1** Brain regions considered in the human connectome according to the AAL parcellation template. The numerical indexes indicate the order in which regions are arranged in **Fig. 1a**. The regions discarded in the graph theoretical analysis in the same way as in Lynall et al. (2010) are indicated in bold.

	Left	Right
<b>Precentral</b>	<b>1</b>	<b>90</b>
Frontal Sup	2	89
Front Sup Orb	3	88
Front Mid	4	87
Front Mid Orb	5	86
Front Inf Ope	6	85
Front Inf Tri	7	84
Front Inf Orb	8	83
Rolandic Oper	9	82
Supp Motor Ar	10	81
<b>Olfactory</b>	<b>11</b>	<b>80</b>
Front Sup Med	12	79
Front Med Orb	13	78
<b>Rectus</b>	<b>14</b>	<b>77</b>
Insula	15	76
Cingulum Ant	16	75
Cingulum Mid	17	74
Cingulum Post	18	73
Hippocampus	19	72
<b>ParaHippocampal</b>	<b>20</b>	<b>71</b>
<b>Amygdala</b>	<b>21</b>	<b>70</b>
Calcarine	22	69
Cuneus	23	68
Lingual	24	67
Occipital Sup	25	66
Occipital Mid	26	65
Occipital Inf	27	64
<b>Fusiform</b>	<b>28</b>	<b>63</b>
Postcentral	29	62
Parietal Sup	30	61
Parietal Inf	31	60
SupraMarginal	32	59
Angular	33	58
Precuneus	34	57
Paracentr Lobule	35	56
Caudate	36	55
Putamen	37	54
Pallidum	38	53
Thalamus	39	52
Heschl	40	51
Temporal Sup	41	50
<b>Temp Pole Sup</b>	<b>42</b>	<b>49</b>
Temporal Mid	43	48
<b>Temp Pole Mid</b>	<b>44</b>	<b>47</b>
<b>Temporal Inf</b>	<b>45</b>	<b>46</b>

### Small-Worldness

A graph  $G$  is considered small-world if its average clustering coefficient  $C(G)$  is significantly higher than for a comparable random graph  $R$  but the mean shortest path length is approximately the same as in a comparable random graph [44,51]. Since the mean shortest path length can be estimated as the inverse of global efficiency [41], small-worldness  $\sigma$  was formulated as follows [32]:

$$\sigma = \frac{C(G)E(G)}{C(R)E(R)}$$

The more  $\sigma$  is higher than 1, the more the graph is considered to be small-world.

### Robustness

Robustness indicates the network's resilience to the removal of nodes. When a node is removed, either randomly (random attack) or in order of higher degree (targeted attack), the network can fragment into 2 or more independent subgraphs. To estimate the robustness of a network, each time a node was removed from the network, we recalculated the size of the largest connected component,  $s$ . Plotting the size  $s(n)$  vs. the number of nodes removed,  $n$ , the robustness parameter is defined as the area under this curve [52]. More robust networks retain a larger connected component even when a large proportion of nodes have been eliminated. To take into account the size of the network, we normalized this value by  $N(N-1)/2$ , so that the maximum robustness is 1.

### Hierarchy

The hierarchy coefficient  $\beta$  is the (positive) exponent of the power-law relationship between the clustering  $C_i$  and the degree  $d_i$  of the nodes in the network such that  $C \sim d^{-\beta}$  [42,43].  $\beta$  was estimated using the least-squares nonlinear fitting function from Matlab®. The more the hierarchy coefficient is high, the more network hubs – defined so for having a large degree – have low clustering, meaning that they are more connected to nodes poorly connected to each other.

### References

- 1 Friston KJ. Theoretical neurobiology and schizophrenia. *Br Med Bull* 1996; 52: 644–655
- 2 Friston KJ, Frith CD. Schizophrenia: a disconnection syndrome? *Clin Neurosci* 1995; 3: 89–97
- 3 Bluhm RL, Miller J, Lanius RA et al. Spontaneous low-frequency fluctuations in the BOLD signal in schizophrenic patients: anomalies in the default network. *Schizophr Bull* 2007; 33: 1004–1012
- 4 Liang M, Zhou Y, Jiang T et al. Widespread functional disconnectivity in schizophrenia with resting-state functional magnetic resonance imaging. *Neuroreport* 2006; 17: 209–213
- 5 Winterer G, Ziller M, Dorn H et al. Schizophrenia: reduced signal-to-noise ratio and impaired phase-locking during information processing. *Clin Neurophysiol* 2000; 111: 837–849
- 6 Friston KJ. Schizophrenia and the disconnection hypothesis. *Acta Psychiatr Scand Suppl* 1999; 395: 68–79
- 7 Winterer G, Weinberger DR. Genes, dopamine and cortical signal-to-noise ratio in schizophrenia. *Trends Neurosci* 2004; 27: 683–690
- 8 Winterer G. Cortical microcircuits in schizophrenia – The dopamine hypothesis revisited. *Pharmacopsychiatry* 2006; 39: S68–S71
- 9 Winterer G. Why do patients with schizophrenia smoke? *Curr Opin Psychiatr* 2010; 23: 112–119
- 10 Mobascher A, Warbrick T, Brinkmeyer J et al. Nicotine effects on attention in schizophrenia: a simultaneous EEG-fMRI study. *Eur Neuropsychopharm* 2011; 21: S515–S516
- 11 Skudlarski P, Jagannathan K, Anderson K et al. Brain connectivity is not only lower but different in schizophrenia: a combined anatomical and functional approach. *Biol Psychiatry* 2010; 68: 61–69
- 12 Mitelman SA, Newmark RE, Torosjan Y et al. White matter fractional anisotropy and outcome in schizophrenia. *Schizophr Res* 2006; 87: 138–159
- 13 Lim KO, Hedehus M, Moseley M et al. Compromised white matter tract integrity in schizophrenia inferred from diffusion tensor imaging. *Arch Gen Psychiatry* 1999; 56: 367–374
- 14 Zalesky A, Fornito A, Seal ML et al. Disrupted axonal fiber connectivity in schizophrenia. *Biol Psychiatry* 2011; 69: 80–89



- 15 Biswal B, Yetkin FZ, Haughton VM *et al.* Functional connectivity in the motor cortex of resting human brain using echo-planar MRI. *Magn Reson Med* 1995; 34: 537–541
- 16 Greicius MD, Supekar K, Menon V *et al.* Resting-state functional connectivity reflects structural connectivity in the default mode network. *Cereb Cortex* 2009; 19: 72–78
- 17 Honey CJ, Sporns O, Cammoun L *et al.* Predicting human resting-state functional connectivity from structural connectivity. *Proc Natl Acad Sci USA* 2009; 106: 2035–2040
- 18 Lynall ME, Bassett DS, Kerwin R *et al.* Functional connectivity and brain networks in schizophrenia. *J Neurosci* 2010; 30: 9477–9487
- 19 Sporns O, Chialvo DR, Kaiser M *et al.* Organization, development and function of complex brain networks. *Trends Cogn Sci* 2004; 8: 418–425
- 20 Shenton ME, Dickey CC, Frumin M *et al.* A review of MRI findings in schizophrenia. *Schizophr Res* 2001; 49: 1–52
- 21 Knöchel C, Oertel-Knöchel V, Schönmeier R *et al.* Interhemispheric hypoconnectivity in schizophrenia: Fiber integrity and volume differences of the corpus callosum in patients and unaffected relatives. *Neuroimage* 2012; 59: 926–934
- 22 Konrad A, Winterer G. Disturbed structural connectivity in schizophrenia – Primary factor in pathology or epiphenomenon? *Schizophrenia Bull* 2008; 34: 72–92
- 23 Hoptman MJ, Ardekani BA, Butler PD *et al.* DTI and impulsivity in schizophrenia: a first voxelwise correlational analysis. *Neuroreport* 2004; 15: 2467–2470
- 24 Skelly LR, Calhoun V, Meda SA *et al.* Diffusion tensor imaging in schizophrenia: relationship to symptoms. *Schizophr Res* 2008; 98: 157–162
- 25 Cabral J, Hugues E, Sporns O *et al.* Role of local network oscillations in resting-state functional connectivity. *Neuroimage* 2011; 57: 130–139
- 26 Gong G, Rosa-Neto P, Carbonell F *et al.* Age- and gender-related differences in the cortical anatomical network. *J Neurosci* 2009; 29: 15684–15693
- 27 Tzourio-Mazoyer N, Landeau B, Papathanassiou D *et al.* Automated anatomical labeling of activations in SPM using a macroscopic anatomical parcellation of the MNI MRI single-subject brain. *Neuroimage* 2002; 15: 273–289
- 28 Jenkinson M, Bannister P, Brady M *et al.* Improved optimization for the robust and accurate linear registration and motion correction of brain images. *Neuroimage* 2002; 17: 825–841
- 29 Collins D, Neelin P, Peters T *et al.* Automatic 3D intersubject registration of MR volumetric data in standardized Talairach space. *J Comput Assist Tomography* 1994; 18: 192–205
- 30 Behrens TE, Woolrich MW, Jenkinson M *et al.* Characterization and propagation of uncertainty in diffusion-weighted MR imaging. *Magn Reson Med* 2003; 50: 1077–1088
- 31 Behrens TE, Berg HJ, Jbabdi S *et al.* Probabilistic diffusion tractography with multiple fibre orientations: What can we gain? *Neuroimage* 2007; 34: 144–155
- 32 Achard S, Bullmore E. Efficiency and cost of economical brain functional networks. *PLoS Comput Biol* 2007; 3: e17
- 33 Bartos M, Vida I, Jonas P. Synaptic mechanisms of synchronized gamma oscillations in inhibitory interneuron networks. *Nat Rev Neurosci* 2007; 8: 45–56
- 34 Brunel N. Dynamics of sparsely connected networks of excitatory and inhibitory spiking neurons. *J Comput Neurosci* 2000; 8: 183–208
- 35 Brunel N, Wang XJ. What determines the frequency of fast network oscillations with irregular neural discharges? I. Synaptic dynamics and excitation-inhibition balance. *J Neurophysiol* 2003; 90: 415–430
- 36 Borgeers C, Kopell N. Synchronization in networks of excitatory and inhibitory neurons with sparse, random connectivity. *Neural Comput* 2003; 15: 509–538
- 37 Acebron JA, Bonilla LL, Vicente CJP *et al.* The Kuramoto model: A simple paradigm for synchronization phenomena. *Rev Mod Phys* 2005; 77: 137–185
- 38 Friston KJ, Harrison L, Penny W. Dynamic causal modelling. *Neuroimage* 2003; 19: 1273–1302
- 39 Shanahan M. Metastable chimera states in community-structured oscillator networks. *Chaos* 2010; 20
- 40 Tononi G, Sporns O, Edelman GM. A measure of brain complexity: relating functional segregation and integration in the nervous system. *Proc Natl Acad Sci U S A* 1994; 91: 5033–5037
- 41 Latora V, Marchiori M. Efficient behavior of small-world networks. *Phys Rev Lett* 2001; 87: 198701
- 42 Ravasz E, Barabasi AL. Hierarchical organization in complex networks. *Phys Rev E Stat Nonlin Soft Matter Phys* 2003; 67: 026112
- 43 Bassett DS, Bullmore E, Verchinski BA *et al.* Hierarchical organization of human cortical networks in health and schizophrenia. *J Neurosci* 2008; 28: 9239–9248
- 44 Watts DJ, Strogatz SH. Collective dynamics of 'small-world' networks. *Nature* 1998; 393: 440–442
- 45 Rubinov M, Sporns O. Complex network measures of brain connectivity: uses and interpretations. *Neuroimage* 2010; 52: 1059–1069
- 46 Friston KJ. The disconnection hypothesis. *Schizophr Res* 1998; 30: 115–125
- 47 Stephan KE, Baldeweg T, Friston KJ. Synaptic plasticity and disconnection in schizophrenia. *Biol Psychiatry* 2006; 59: 929–939
- 48 Coyle JT, Tsai G, Goff D. Converging evidence of NMDA receptor hypofunction in the pathophysiology of schizophrenia. *Ann N Y Acad Sci* 2003; 1003: 318–327
- 49 Supekar K, Menon V, Rubin D *et al.* Network analysis of intrinsic functional brain connectivity in Alzheimer's disease. *Plos Comput Biol* 2008; 4: e1000100
- 50 Boccaletti S, Latora V, Moreno Y *et al.* Complex networks: Structure and dynamics. *Physics Reports* 2006; 424: 175–308
- 51 Humphries MD, Gurney K, Prescott TJ. The brainstem reticular formation is a small-world, not scale-free, network. *Proc Biol Sci* 2006; 273: 503–511
- 52 Achard S, Salvador R, Whitcher B *et al.* A resilient, low-frequency, small-world human brain functional network with highly connected association cortical hubs. *J Neurosci* 2006; 26: 63–72